OPEN ACCESS Freely available online

PLOS ONE

The LDL-HDL Profile Determines the Risk of Atherosclerosis: A Mathematical Model

Wenrui Hao[1]*, **Avner Friedman**[2]

1 Mathematical Biosciences Institute, The Ohio State University, Columbus, Ohio, United States of America, **2** Mathematical Biosciences Institute & Department of Mathematics, The Ohio State University, Columbus, Ohio, United States of America

Abstract

Atherosclerosis, the leading death in the United State, is a disease in which a plaque builds up inside the arteries. As the plaque continues to grow, the shear force of the blood flow through the decreasing cross section of the lumen increases. This force may eventually cause rupture of the plaque, resulting in the formation of thrombus, and possibly heart attack. It has long been recognized that the formation of a plaque relates to the cholesterol concentration in the blood. For example, individuals with LDL above 190 mg/dL and HDL below 40 mg/dL are at high risk, while individuals with LDL below 100 mg/dL and HDL above 50 mg/dL are at no risk. In this paper, we developed a mathematical model of the formation of a plaque, which includes the following key variables: LDL and HDL, free radicals and oxidized LDL, MMP and TIMP, cytockines: MCP-1, IFN-γ, IL-12 and PDGF, and cells: macrophages, foam cells, T cells and smooth muscle cells. The model is given by a system of partial differential equations with in evolving plaque. Simulations of the model show how the combination of the concentrations of LDL and HDL in the blood determine whether a plaque will grow or disappear. More precisely, we create a map, showing the risk of plaque development for any pair of values (LDL,HDL).

Citation: Hao W, Friedman A (2014) The LDL-HDL Profile Determines the Risk of Atherosclerosis: A Mathematical Model. PLoS ONE 9(3): e90497. doi:10.1371/journal.pone.0090497

Editor: Xiao-Feng Yang, Temple University School of Medicine, United States of America

Received December 20, 2013; **Accepted** February 3, 2014; **Published** March 12, 2014

Funding: This research has been supported by the Mathematical Biosciences Institute and the National Science Foundation under grant DMS 0931642 (http://nsf.gov/awardsearch/showAward?AWD_ID = 0931642). The funders had no role in study design, data collection and analysis, decision to publish, or preparation of the manuscript.

Competing Interests: The authors have declared that no competing interests exist.

* E-mail: hao.50@mbi.osu.edu

Introduction

Atherosclerosis, hardening of the arteries, is the leading cause of death in the United States, and worldwide. The disease triggers heart attack or stroke, with total annual death of 900,000 in the United States [1] and 13 million worldwide [2].

Atherosclerosis is a disease in which a plaque builds up inside the arteries. A plaque contains low density lipoprotein (LDL), macrophages, smooth muscle cells (SMCs), platelets, and debris. The plaque constricts the lumen of the blood vessel thereby increasing the shear force of blood flow [3,4]. As the plaque continues to grow, the increased shear force may cause rupture of the plaque, possibly resulting in the formation of thrombus (blood clot) [3,5], ischemic stroke, and heart attack [3–5].

The process of plaque development begins with a lesion in the endothelial layer, allowing LDL, to move from the blood into the intima and becoming oxidized LDL (ox-LDL) by free radicals (FRs). FRs are oxidative agents continuously released by biochemical reactions within the body, including the intima [6–8]. Endothelial cells, sensing the presence of ox-LDL, secrete monocyte chemoattractant protein (MPC-1) [9,10], which triggers recruitment of monocytes into the intima [11]. After entering the intima, monocytes differentiate into macrophages, which have an affinity for the ox-LDL [12–14]. The ingestion of large amounts of ox-LDL transforms the fatty macrophages into foam cells [12,15]. Foam cells secrete chemokines which attract more macrophages [10,12,13]. SMCs from the media move into the intima by chemotactic forces due to MCP-1 [9,10], and platelet-derived growth factor (PDGF) [10,16], as well as by haptotaxis by the extracellular matrix (ECM). PDGF is secreted by macrophages, foam cells and SMCs [16,17]. ECM is remodeled by matrix metalloproteinase (MMP) produced by a variety of cell types including SMCs [18], and is inhibited by tissue inhibitor of metalloproteinase (TIMP) produced by macrophages and SMCs [19]. Interleukin IL-12, secreted by macrophages and foam cells [10,12,20], contribute to the growth of a plaque by activating T cells [9,20,21]. Indeed, the activated T cells secrete interferon IFN-γ, which in turn activates macrophage in the intima [13,21,22]. At the same time that LDL enters the intima, high density lipoprotein (HDL) also enters into the intima, and becomes oxidized by free radicals [7,8]. However, oxidized HDL (ox-HDL) is not ingested by macrophages. HDL helps prevent atherosclerosis by removing cholesterol from foam cells, and by the limiting inflammatory processes that underline atherosclerosis [23]. Furthermore, HDL takes up free radicals that are otherwise available to LDL. Some of the key players in the atherosclerosis process are shown in Fig. 1.

It has long been recognized that the cholesterol concentrations in the blood are indicators of the probability that a plaque will develop: higher LDL and lower HDL concentrations indicate a higher probability of plaque development. Public health guidelines in the U.S. specify what levels of LDL are low risk and what levels are high risk; they also specify what levels of HDL are poor and what levels are near ideal [24,25]. However, what is more relevant is to specify the risk associated with combined levels of LDL and HDL, and this is what the present paper addresses. A schematic of

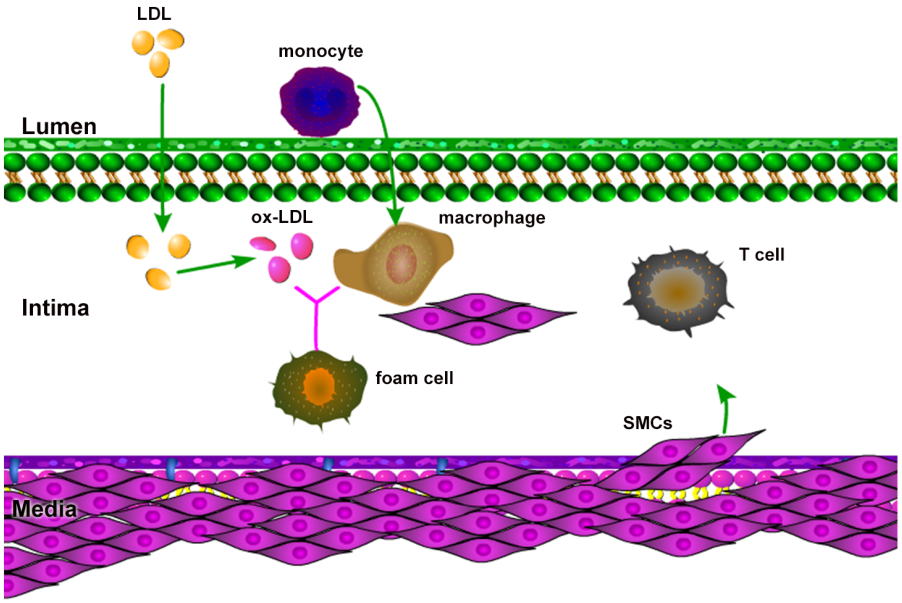

Figure 1. Atherosclerosis schematics: the presence of ox-LDL in the intima causes monocytes to migrate from the lumen into the intima. Monocytes differentiate into macrophages which endocytose ox-LDL and become foam cells. SMCs are attracted from the media into intima by chemotaxis and haptotaxis. Cytokines released by macrophages, foam cells and SMCs activate T cells. T cells enhance activation of macrophages. HDL helps prevent atherosclerosis.
doi:10.1371/journal.pone.0090497.g001

the network of atherosclerosis is given in Fig. 2. In this paper, we developed a mathematical model of plaque formation by a system of partial differential equations based on Fig. 2. The aim of the model is to determine the risk of plaque formation for combined levels of LDL and HDL. In particular, we created a "risk-map" for plaque development in the LDL-HDL coordinate plane, where the first quadrant of the plane was divided into regions of high risk, low risk and no risk. Anti-cholesterol drugs are aimed at lowering high levels of LDL, but some drugs are known to also increase the level of HDL [24]. Hence such a risk-map may be important when evaluating the extend to which an anti-cholesterol drug can reduce the risk of atherosclerosis for particular individuals.

Materials and Methods

Mathematical model

In this paper, we present a mathematical model based on the network shown in Fig. 2. The model includes the variables listed in Table 1. We assume that all cells are moving with a common velocity $\mathbf{u}$; the velocity is the result of movement of macrophages, T cells and SMCs into the intima. We also assume that all species are diffusing with appropriate diffusion coefficients. The equation for each species of cells X has a form

$$\frac{dX}{dt}+\nabla\cdot(\mathbf{u}X)-D_X\Delta X=F_X,$$

where the expression on the left-hand side includes advection and diffusion, and F_X accounts for various growth factors, bio-chemical reactions, chemotaxis and haptotaxis. The equation for the chemical species are the same but without the advection term. Fig. 3 shows a 2D cross section of a blood vessel with plaque Ω, and a planar cross section of a plaque in the direction along a blood vessel.

Equations for lipoproteins [LDL (L), HDL (H), ox-LDL (L_{ox})] and free radical (r). The distribution of LDL, HDL, ox-LDL and free radicals in the intima are described using reaction-diffusion equations [7],

$$\frac{\partial L}{\partial t}-D_L\Delta L=\underbrace{-k_LrL}_{reduction}, \tag{1}$$

$$\frac{\partial H}{\partial t}-D_H\Delta H=\underbrace{-k_HrH}_{reduction}, \tag{2}$$

$$\frac{\partial L_{ox}}{\partial t}-D_{L_{ox}}\Delta L_{ox}=\underbrace{k_LrL}_{production}\ \underbrace{-\lambda_{L_{ox}M}ML_{ox}}_{reduction}, \tag{3}$$

$$\frac{\partial r}{\partial t}-D_r\Delta r=r_0\underbrace{-r(k_LL+k_HH)}_{reduction}, \tag{4}$$

where k_L and k_H are reaction rates of oxidization, and $\lambda_{L_{ox}M}$ is the reduction rate of ox-LDL due to ingestion by macrophages. Eqs. (1) and (2) model the evolution of LDL and HDL concentrations. It is assumed that LDL and HDL are lost by reaction of oxidation with free radicals. Equation (3) models the production of ox-LDL due to LDL oxidation by reaction with the radicals (first term on right-hand side) and a reduction of ox-LDL through ingestion by macrophages (second term on right-hand side). Equation (4) models the evolution of free radicals concentration with baseline growth r_0.

Equation for macrophages (M). The evolution of macrophage density is modeled by

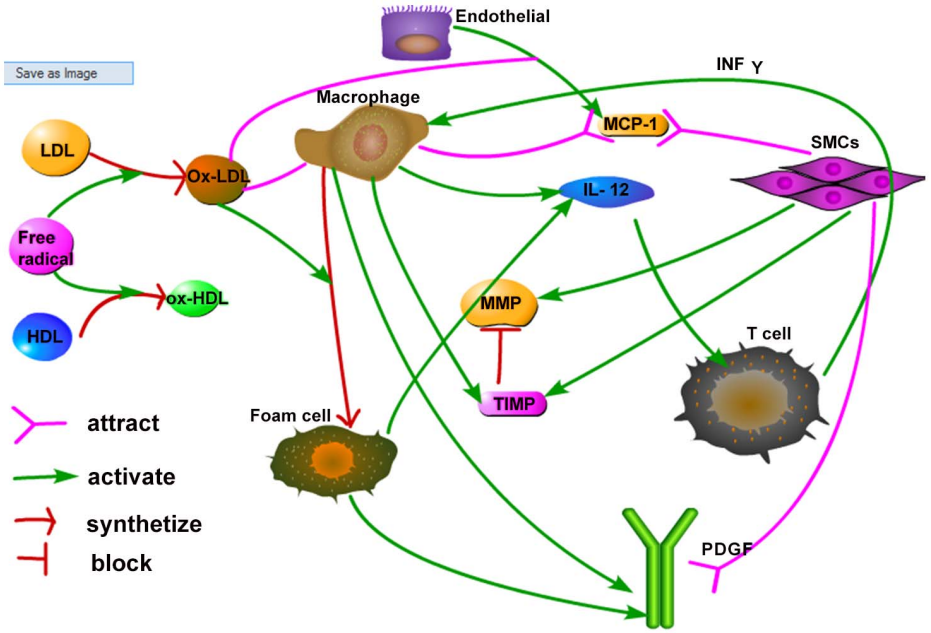

Figure 2. Schematic network of atherosclerosis. LDL and HDL are oxidized by free radicals, and become ox-LDL and ox-HDL respectively. Ox-LDL recruits macrophages to intima. By ingesting ox-LDL, macrophages are transformed to foam cells. SMCs are attracted into the intima by MCP-1 (secreted by endothelial cells) and PDGF (secreted by macrophages and foam cells). Macrophages, foam cells and SMCs secrete IL-12, which activates T cells. IFN-γ secreted by T cells enhance the activity of macrophages which contributes the plaque built-up.
doi:10.1371/journal.pone.0090497.g002

$$\frac{\partial M}{\partial t}+\nabla\cdot(\mathbf{u}M)-D_M\Delta M=\underbrace{-\nabla\cdot(M\chi_C\nabla P)}_{chemotaxis}+\underbrace{\lambda_{MI_\gamma}M\frac{I_\gamma}{I_\gamma+K_{I_\gamma}}}_{activation}\underbrace{-d_M M}_{death}. \quad (5)$$

Here the first term on right-hand side accounts for recruitment of macrophages by MCP-1 [9], and the second term accounts for the activation of macrophages by IFN-γ [13,21,22].

Equation for MCP-1 (P). The MCP-1 equation is given by

$$\frac{\partial P}{\partial t}-D_P\Delta P=\underbrace{\lambda_{PE}\frac{L_{ox}}{K_{L_{ox}}+L_{ox}}}_{production}\underbrace{-d_P P}_{degradation}, \quad (6)$$

where the first term on the right-hand side is the production of MCP-1 by endothelial cells, whose density is assumed to be constant, under the influence of ox-LDL [9].

Equation for T cells (T). The density of T cells, which are primarily $CD4^+$ T cells [20], satisfies the equation

$$\frac{\partial T}{\partial t}+\nabla\cdot(\mathbf{u}T)-D_T\Delta T=\underbrace{\lambda_{TI_{12}}\frac{M}{K_M+M}I_{12}}_{activtion}\underbrace{-d_T T}_{death}. \quad (7)$$

In this equation, we assume that T cells are activated by IL-12 in conjunction with MHC-II (major histocompatibility complex, class II). Actually, T cells are also activated by IL-1 and IL-6 produced by macrophages and SMCs [10,12,13]. However, because of lack of experimental data, we do not include the IL-1 and IL-6 explicitly but instead consider their effect implicitly in estimating

Table 1. The variables of the model: concentrations and densities are in units of g/cm^3.

L:	concentration of LDL	H:	concentration of HDL
L_{ox}:	concentration of ox-LDL	r:	concentration of free radicals
P:	concentration of MCP-1	I_γ:	concentration of IFN-γ
I_{12}:	concentration of IL-12	G:	concentration of PDGF
Q:	concentration of MMPs	Q_r:	concentration of TIMP
M:	density of macrophages	T:	density of T cells
S:	density of SMCs	ρ:	density of ECM
F:	density of foam cell	σ:	pressure (in $g\ cm^2/day$)
$\mathbf{u}$:	fluid velocity (in cm/day)		

doi:10.1371/journal.pone.0090497.t001

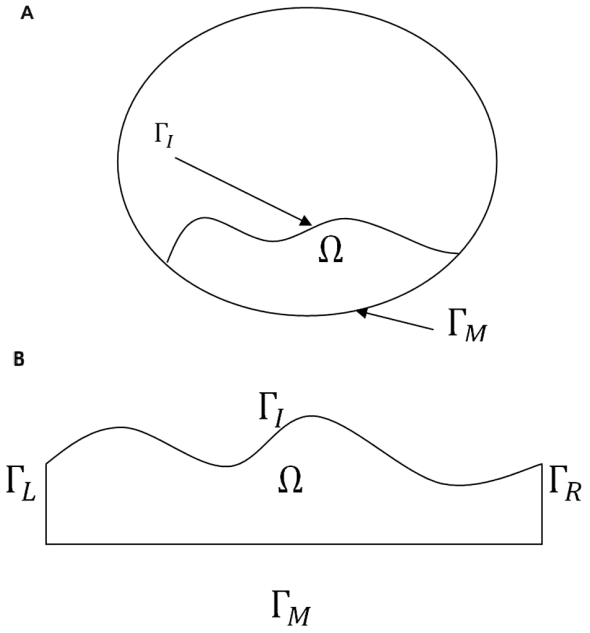

Figure 3. Two 2D cross sections of a plaque. Γ_M is the boundary of the intima in contact with the media, and Γ_I is the boundary of the intima in contact with the lumen. In (B) Γ_L and Γ_R are parts of the intima.
doi:10.1371/journal.pone.0090497.g003

the parameter $\lambda_{TI_{12}}$. For simplicity, we include the anti-inflammatory effect of IL-10 produced by macrophages only implicitly, by the factor $1/(K_M+M)$.

Equation for IFN-γ (I_γ). The dynamics of IFN-γ concentration is modeled by

$$\frac{\partial I_\gamma}{\partial t} - D_{I_\gamma}\Delta I_\gamma = \underbrace{\lambda_{I_\gamma T} T}_{production}\ \underbrace{-d_{I_\gamma} I_\gamma}_{degradation}, \tag{8}$$

where the first term on right-hand side represents production of I_γ by T cells [21].

Equation for SMCs (S). The equation of the SMCs density is given by

$$\frac{\partial S}{\partial t} + \nabla\cdot(\mathbf{u}S) - D_S\Delta S = \underbrace{-\nabla\cdot(S\chi_C\nabla P) - \nabla\cdot(S\chi_C\nabla G)}_{chemotaxis}\ \underbrace{-\nabla\cdot(S\chi_H\nabla\rho)}_{haptotaxis}. \tag{9}$$

The first two terms on right-hand side account for chemotaxis by MCP-1 [9,10], and PDGF [10,16], and the last term accounts for haptotaxis by ECM.

Equation for IL-12 (I_{12}). The concentration of IL-12 is modeled by

$$\frac{\partial I_{12}}{\partial t} - D_{I_{12}}\Delta I_{12} = \underbrace{\lambda_{I_{12}M}\frac{M}{K_M+M}\left(1+\frac{I_\gamma}{K_{I_{12}}H+I_\gamma}\right)+\lambda_{I_{12}F}\frac{F}{K_F+F}}_{production}\ \underbrace{-d_{I_{12}}I_{12}}_{degradation}. \tag{10}$$

The first term of right-hand side is the production of I_{12} by macrophages enhanced by I_γ and resisted by HDL [23]. The production of I_{12} by macrophages is resisted by I_{10} (which, for simplicity, is accounted by the factor $\frac{1}{K_M+M}$) [10,12]. The second term represents the production of I_{12} by foam cells [20].

Equations for PDGF (G), MMP (Q) and TIMP (Q_r). We have the following sets of reaction diffusion equations for the chemokines (G, Q and Q_r):

$$\frac{\partial G}{\partial t} - D_G\Delta G = \underbrace{\lambda_{GM}M+\lambda_{GF}F+\lambda_{GS}S}_{production}\ \underbrace{-d_G G}_{degradation} \tag{11}$$

$$\frac{\partial Q}{\partial t} - D_Q\Delta Q = \underbrace{\lambda_{QS}S}_{production}\ \underbrace{-d_{QQ_r}Q_rQ}_{depletion}\ \underbrace{-d_Q Q}_{degradation} \tag{12}$$

$$\frac{\partial Q_r}{\partial t} - D_{Q_r}\Delta Q_r = \underbrace{\lambda_{Q_rS}S+\lambda_{Q_rM}M}_{production}\ \underbrace{-d_{Q_rQ}QQ_r}_{depletion}\ \underbrace{-d_{Q_r}Q_r}_{degradation} \tag{13}$$

In equation (11), PDGF is produced by macrophages, foam cells, and SMCs [16,17]. In equation (12), MMP is secreted by SMCs [18] (first term on right-hand side), and is lost by binding with TIMP (second term). In equation (13), TIMP is produced by SMCs and macrophages [19].

Equation for foam cells (F). Macrophages that have ingested a large amount of ox-LDL become foam cells [7,12,15], so we have

$$\frac{\partial F}{\partial t} + \nabla\cdot(\mathbf{u}F) - D_F\Delta F = \underbrace{\lambda_{FM}\frac{L_{ox}}{K_{L_{ox}}+L_{ox}}M}_{production}\ \underbrace{-d_F F}_{death}. \tag{14}$$

Equations for ECM (ρ) and pressure (σ). We assume that the intima has the constituency of a porous medium. Then, by Darcy's law, the velocity $\mathbf{u}$ of the cells is given by

$$\mathbf{u} = -\nabla\sigma, \tag{15}$$

where σ is the pressure. We also assume that the total density of all the cells plus the concentration of ρ is constant. This constant should be smaller than the average density of a plaque, 1.22 ± 0.03 g/cm^3 [26], because plaques contain some debris, which are not included in our model. We take the constant to be 1 g/cm^3, i.e.,

$$M+F+T+S+\rho = 1. \tag{16}$$

We assume that all cells are approximately of the same volume and surface area, so that the diffusion coefficients of the all cells have the same coefficient, D. By adding Eqs. (5), (7), (9) and (14), we get

$$-\frac{\partial\rho}{\partial t} - (1-\rho)\Delta\sigma + \nabla\sigma\cdot\nabla\rho + D\Delta\rho = \phi \tag{17}$$

where

$$\begin{aligned}\phi = &-\nabla\cdot(M\chi_C\nabla P)+\lambda_{MI_\gamma}M\frac{I_\gamma}{I_\gamma+K_{I_\gamma}}-d_M M\\ &+\lambda_{TI_{12}}\frac{M}{K_M+M}I_{12}-d_T T-\nabla\cdot(S\chi_C\nabla P)\\ &-\nabla\cdot(S\chi_C\nabla G)-\nabla\cdot(S\chi_H\nabla\rho)\\ &+\lambda_{FM}\frac{L_{ox}}{K_{L_{ox}}+L_{ox}}M-d_F F.\end{aligned} \tag{18}$$

Eq. (17) gives a relation between ρ and σ. We next derive an equation for ρ. The ECM is degraded by MMP [27], and is remodeled by macrophages and SMCs [18,27]. For simplicity, we take the remodeling rate to be a constant, λ_ρ, as in [28]. Then the equation of the density of ECM is given by

$$\frac{\partial\rho}{\partial t}+\nabla\cdot(\mathbf{u}\rho)=\lambda_\rho\rho(1-\frac{\rho}{\rho_0})\underbrace{-d_{\rho Q}Q\rho}_{degradation}. \tag{19}$$

Since $u=-\nabla\sigma$, this equation can be written in the form

$$\frac{\partial\rho}{\partial t}-\rho\Delta\sigma-\nabla\sigma\cdot\nabla\rho=\psi,$$

where

$$\psi=\lambda_\rho\rho(1-\frac{\rho}{\rho_0})-d_{\rho Q}Q\rho. \tag{20}$$

Adding this equation and (17), we get our final equation for σ:

$$-\Delta\sigma+D\Delta\rho=\phi+\psi. \tag{21}$$

The equation for ρ can then be written as

$$\frac{\partial\rho}{\partial t}-D\rho\Delta\rho+(\phi+\psi)\rho-\nabla\sigma\cdot\nabla\rho=\psi. \tag{22}$$

Boundary conditions

For simplicity, we consider only 2-dimensional plaques as in Fig. 3. Then the boundary of the plaque consists of i) Γ_M, in contact with media; ii) a free boundary Γ_I, inside the lumen, and iii) two more vertical boundaries Γ_L and Γ_R of the intima in the case of Fig. 3(B).

Boundary conditions on Γ_I. We assume flux boundary conditions of the form

$$\frac{\partial X}{\partial\mathbf{n}}+\alpha_X(X-X_0)=0 \tag{23}$$

for $X=L$, H, M, T, and non-flux boundary conditions for all other variables,

$$\frac{\partial Y}{\partial\mathbf{n}}=0, \tag{24}$$

where $Y=L_{ox}$, r, P, I_γ, S, I, I_{12}, G, Q, Q_r, F. The boundary values for ρ are determined by Eq. (16). The coefficient α_X is a constant except for M, and $\alpha_M(L_{ox},H)=\tilde{\alpha}_M\frac{L_{ox}}{1+H}$, since ox-LDL attracts monocytes [11], while HDL limits the inflammation process[23]. Note that L_0 and H_0 are the LDL and HDL concentrations in the blood, so we shall be interested to see how these concentrations determine whether a small plaque will grow or shrink.

As in [29–31], we assume that the free boundary Γ_I is held together by cell-to-cell adhesion forces so that

$$\sigma=\gamma\kappa \text{ on } \Gamma_I,$$

where κ is the mean curvature of the surface Γ_I. (If Γ_I is circular, then κ is the reciprocal of the radius) Furthermore, the continuity condition $\mathbf{u}\cdot\mathbf{n}=V_n$, where $\mathbf{n}$ is the outward normal and V_n is the velocity of the free boundary Γ_I in the direction $\mathbf{n}$, yields the relation

$$V_n=-\frac{\partial\sigma}{\partial\mathbf{n}} \text{ on } \Gamma_I. \tag{25}$$

Boundary conditions on Γ_M. We assume non-flux boundary conditions for all variables except ρ and S on Γ_M: For S, we have

$$\frac{\partial S}{\partial\mathbf{n}}+\alpha_S(S-S_0)=0, \text{ on } \Gamma_M$$

where S_0 is SMCs density in the media, and for simplicity we take $\alpha_S=\alpha_S(P,G)=\tilde{\alpha}_S\frac{P+G}{P_0+G_0}$ since MCP-1 and PDGF attract SMCs from the media. As in the case of Γ_I, the boundary values of ρ are determined by Eq. (16).

Boundary conditions on Γ_L and Γ_R. We assume the periodic boundary conditions on Γ_L and Γ_R.

Parameter estimation

Table 2 lists the range of molecular weights of proteins and Table 3 lists their range of concentration. In the second columns in Tables 2 and 3, we indicate the (intermediate) values used in the simulations. The Tables 2 and 3 are used to estimate some of the model parameters. A summary of all the model parameters is given in Tables 4 and 5.

Reaction rates. To estimate some of the parameters in the equations for proteins, we shall use the concept of "accessible surface area" [32,33] of a protein p, or briefly "area," A_p, which is roughly the minimum surface area of the smooth shapes containing the protein. It was estimated in [34], that $A_{LDL}=1.02\times10^{-11}\ cm^2$, and $A_{HDL}=1.34\times10^{-12}\ cm^2$, so that their ratio is

$$R_{LH}=\frac{A_{LDL}}{A_{HDL}}=7.6.$$

Accordingly, the corresponding reaction rates of the oxidation, k_L and k_H, are related by $k_L=7.6k_H$. Moreover, the reaction rate of oxidation of LDL by free radicals is $k_L=10.37\ gcm^{-3}\ \text{day}^{-1}$ [7,34,35], so that $k_H=1.36$ g $cm^{-3}\ \text{day}^{-1}$.

Diffusion coefficients. We assume that the diffusion coefficients of all the cells are the same, and take them to be $8.64\times10^{-7}\ cm^2\ \text{day}^{-1}$ [28,36]. In order to estimate the diffusion coefficients of the various proteins, we assume that the diffusion coefficient of protein p, D_p, is proportional to its area A_p, i.e., $D_p=KA_p$, where we take K to be the same for all small molecules. For glucose, which is a monomeric globular protein, A_p can be

Table 2. Molecular weights.

Protein	Weight (kda)	Explanation
LDL	549	Over 95% of the LDL protein mass is apolipoprotein
		B-100 (apo B-100, 549 kDa (1000 g/mol)) [63].
HDL	105	The range of weight of HDL is 105–130 [64].
Free radical	0.51 kda	Free radicals include DPPH (0.39 kda),
		ABTS (0.51 kda) and superoxide anion (0.81 kda) [65].
IFN-γ	17	IFN-γ is described as a 17 kDa peptide [66].
PDGF	35	There are two PDGF polypeptides:
		PDGF-I with a molecular weight of about 35 kda, and
		PDGF-II with a molecular weight of about 32 kda [67].
MCP-1	8.9	[68]
IL-12	70	[69]
MMP	52	MMP-1 has two major species of molecular
		mass, 57 kDa and 52 kDa [48].
TIMP	25	The molecular weights of TIMP-1, TIMP-2 and TIMP-3
		are 28.5 kDa 21 kDa and 27 kDa respectively [48].

doi:10.1371/journal.pone.0090497.t002

computed in terms of the molecular weight M_p, by the formula $A_p = 11.1 M_p^{2/3}$ [33], and $M_p = 180$ dalton [28], $D_p = 1.04 \times 10^{-1}\ cm^2\ \text{day}^{-1}$ [37]. Hence, for glucose, K is determined by

$$\begin{aligned} K &= \frac{\text{diffusion coefficient of glucose}}{\text{surface area of glucose}} \\ &= \frac{\text{diffusion coefficient of glucose}}{11.1 M_p^{2/3}} \\ &= \frac{1.04 \times 10^{-1}\ cm^2\ day^{-1}}{11.1 \times (180)^{2/3} \times 10^{-16}\ cm^2} = 2.93 \times 10^{12}\ day^{-1}. \end{aligned} \tag{26}$$

We can now compute $D_L = KA_{LDL} = 2.93 \times 10^{12} \times 1.02 \times 10^{-11} = 29.89\ cm^2\ \text{day}^{-1}$ and $D_H = KA_{HDL} = 3.93\ cm^2\ \text{day}^{-1}$. Free radicals are monomeric globular proteins (average weight is 500 da, Table 2). Hence

$$\begin{aligned} D_r &= KA_{\text{free radicals}} = K \times 11.1 \times M_{\text{free radicals}}^{2/3} \\ &= 2.93 \times 10^{12} \times 11.1 \times (500)^{2/3} \times 10^{-16} = 2.05 \times 10^{-1}\ cm^2\,\text{day}^{-1}. \end{aligned}$$

The diffusion coefficient of MMP is $4.32 \times 10^{-2}\ cm^2\ \text{day}^{-1}$ [38]. We assume that the diffusion coefficient of TIMP is same as that of MMP.

Production rates. We assume that, in Eq. (7), $\lambda_{TI_{12}}[I_{12}] \approx 2d_T[T]$, where $[X]$ denotes the average concentration of X. We take $[I_{12}] \approx 5 \times 10^{-10}\ \text{gcm}^{-3}$, $[T] \approx 1 \times 10^{-3}\ \text{gcm}^{-3}$ from Table 3, and $d_T = 0.33\ \text{day}^{-1}$ [39,40]. Then $\lambda_{TI_{12}}$ is estimated by $1 \times 10^6\ \text{day}^{-1}$.

Table 3. Concentrations of proteins and cells.

Proteins & cells	Concentration (gcm^{-3})	Explanation
LDL	7×10^{-4}–1.9×10^{-3}	Range is 70–190 mg/dl [25,70].
HDL	4×10^{-4}–6×10^{-4}	Range is 40–60 mg/dl [25,70].
IFN-γ	10^{-9}	Range is of 0.1–10.0 ng/mL [10].
PDGF	1.5×10^{-8}	Range in normal humans blood
		17.5±3.1 ng/mL [72].
MCP-1	3×10^{-10}	300 pg/ml [73]
IL-12	5×10^{-10}	Range 200–800 pg/ml [20].
MMP	3×10^{-8}	Range in plasma is 10~60 ng/ml [74].
TIMP	3×10^{-8}	Range in plasma is 10~60 ng/ml [74]
SMC	6×10^{-3}	Range 7,500,000–10,000,000 cells per ml [38].
Monocyte	5×10^{-5}	Range from 20,000 to 100,000 cells per ml [75].
T cell	1×10^{-3}	Range of $CD4^+$ T cells in healthy normal adult
		of 500,000 to 1,500,000 cells per ml [49].

doi:10.1371/journal.pone.0090497.t003

Table 4. Parameters' description and value.

Parameter	Description	Value
k_L	reaction rate of LDL + Radical→ox-LDL	2.35×10^{-4} g^{-1} cm^3 day^{-1} [7,34,35]
k_H	reaction rate of HDL + Radical→ox-HDL	5.29×10^{-6} g^{-1} cm^3 day^{-1} [7,34]
D_L	diffusion coefficient of LDL	29.89 cm^2 day^{-1} [33,34,37] & estimated
D_H	diffusion coefficient of HDL	3.93 cm^2 day^{-1} [33,34,37] & estimated
$D_{L_{ox}}$	diffusion coefficient of oxidized LDL	29.89 cm^2 day^{-1} [33,34,37] & estimated
D_r	diffusion coefficient of radicals	2.05×10^{-1} cm^2 day^{-1} [33,34,37] & estimated
D_M	diffusion coefficient of macrophage	8.64×10^{-7} cm^2 day^{-1} [28,36]
D_T	diffusion coefficient of T-cell	8.64×10^{-7} cm^2 day^{-1} [28,36]
D_{I_γ}	diffusion coefficient of IFN-γ	1.08×10^{2} cm^2 day^{-1} [76]
D_S	diffusion coefficient of SMCs	8.64×10^{-7} cm^2 day^{-1} [28,36]
D_P	diffusion coefficient of MCP-1	17.28 cm^2 day^{-1} [44]
$D_{I_{12}}$	diffusion coefficient of IL-12	1.08×10^{2} cm^2 day^{-1} [76]
D_G	diffusion coefficient of PDGF	8.64×10^{-2} cm^2 day^{-1} [42]
D_Q	diffusion coefficient of MMP	4.32×10^{-2} cm^2 day^{-1} [38]
D_{Q_r}	diffusion coefficient for TIMPs	4.32×10^{-2} cm^2 day^{-1} [33,37,38] & estimated
D_F	diffusion coefficient of foam cells	8.64×10^{-7} cm^2 day^{-1} [28,36]
$\lambda_{L_{ox}M}$	rate of ox-LDL ingestion by macrophages	10 gcm^{-3} day^{-1} [7]
λ_{MI_γ}	activation rate of macrophages by IFN-γ	0.005 day^{-1} [39] & estimated
λ_{PE}	production rate of MCP-1	8.65×10^{-10} gcm^{-3} day^{-1} [44] & estimated
$\lambda_{TI_{12}}$	activation rate of T cells by IL-12	1×10^{6} day^{-1} [39,40,49,74] & estimated
$\lambda_{I_\gamma T}$	production rate of IFN-γ by T cells	0.066 day^{-1} [45,77]
$\lambda_{I_{12}M}$	production rate of IL-12 by macrophages	3×10^{-7} gcm^{-3} day^{-1} [45]
$\lambda_{I_{12}F}$	production rate of IL-12 by foam cells	1×10^{-7} gcm^{-3} day^{-1} [45] & estimated
λ_{GM}	production rate of PDGF by macrophages	0.1 day^{-1} [41,42] & estimated
λ_{GF}	production rate of PDGF by foam cells	0.033 day^{-1} [41,42] & estimated
λ_{GS}	production rate of PDGF by SMCs	0.5 day^{-1} [41,42] & estimated
λ_{QS}	production rate of MMP by SMCs	3×10^{-4} day^{-1} [28]
λ_{Q_rS}	production rate of TIMP by SMCs	3×10^{-5} day^{-1} [28] & estimated
λ_{Q_rM}	production rate of TIMP by macrophages	6×10^{-5} day^{-1} [28] & estimated
λ_ρ	remodeling rate of ECM	0.432 day^{-1} [28]
λ_{FM}	activation rate of foam cells	0.12 day^{-1} [39] & estimated
d_M	death rate of macrophage	0.015 day^{-1} [39]
d_P	degradation rate of MCP-1	1.73 day^{-1} [44]
d_T	death rate of T cell	0.33 day^{-1} [39,40]
d_{I_γ}	degradation rate of IFN-γ	0.69 day^{-1} [37]
d_S	death rate of SMC	0.86 day^{-1} [7]
$d_{I_{12}}$	degradation rate of IL-12	1.188 day^{-1} [39,40]
d_G	degradation rate of PDGF	3.84 day^{-1} [42]
d_{QQ_r}	binding rate of MMP to TIMP	4.98×10^{8} cm^3g^{-1} day^{-1} [44,48] & estimated
d_{Q_rQ}	binding rate of TIMP to MMP	1.04×10^{9} cm^3g^{-1} day^{-1} [44,48] & estimated
d_Q	degradation rate of MMP	4.32 day^{-1} [37]
d_{Q_r}	degradation rate of TIMP	21.6 day^{-1} [46] & estimated
$d_{\rho Q}$	degradation rate of ECM due to MMP	2.59×10^{7} cm^3g^{-1} day^{-1} [36]
d_F	death rate of foam cell	0.03 day^{-1} [39] & estimated

doi:10.1371/journal.pone.0090497.t004

PDGF is produced by SMCs, and likely also by endothelial cells and macrophages [41]. In wound healing, macrophages produce PDGF at rate of 5.76 day^{-1} [42]. Since the plaque formation is a much slower process, we take this rate λ_{GM} to be much smaller, i.e., $\lambda_{GM}=0.1$ day^{-1}. Since SMCs production rate of PDGF is higher than that by macrophages [41], we take $\lambda_{GS}=0.5$ day^{-1}.

The production rate of MMP by tumor cells was estimated in [28] to be 6×10^{-3} day^{-1}. We assume that SMCs produce MMP

at a much lower rate, namely, $\lambda_{QS}=3\times10^{-4}$ day^{-1}. Since SMCs produce MMP to enable them move into the intima by haptotaxis, we assume that they produce TIMP at a lower rate than MMP, and take $\lambda_{Q,S}=\frac{1}{10}\lambda_{QS}=3\times10^{-5}$ day^{-1}. As macrophages produce most of the TIMP [43], we take the production rate of TIMP by macrophages to be $\lambda_{Q,M}=2\lambda_{Q,S}=6\times10^{-5}$ day^{-1}.

We assume that the production rate of MCP-1 by endothelial cells, λ_{PE}, is twice that of $d_P P_0$, where P_0 is the concentration of MCP in the blood, which is equal to 1×10^{-9} gcm^{-3} [44]. We assume that $d_F=\frac{1}{2}d_M=0.03$ day^{-1} [39], and that, in Eq. (14), $\lambda_{FM}[M]\approx4d_F[F]$ and $[F]\approx[M]$, so that $\lambda_{FM}=4d_F=0.12$ day^{-1}.

By [45], $\lambda_{I_{12}M}=3\times10^{-7}$ day^{-1}. We assume that foam cells have lower production rates of I_{12} and PDGF than macrophages, and take $\lambda_{I_{12}F}$ and λ_{GF} to be one third of the values of $\lambda_{I_{12}M}$ and λ_{GM}, respectively, so that $\lambda_{I_{12}F}=1\times10^{-7}$ gcm^{-3} day^{-1}, and $\lambda_{GF}=0.033$ day^{-1}.

Degradation rates. The degradation rate of MMP is $d_Q=4.32$ day^{-1} [37]. Since TIMP has a short half life compared to MMP [46], we take its degradation rate to be $d_{Q_r}=5d_Q=21.6$ day^{-1}.

In [47], the binding rate of MMP and TIMP is reported to be 3×10^5 $M^{-1}s^{-1}$, where $1M=$the mass per mole, and the molecular weights of MMP and TIMP are 52 kda and 25 kda, respectively [48]. Accordingly, we derive the binding rate per Molar per second (by same formula as in [44]),

$$d_{QQ_r}=\frac{3.0\times10^5}{\frac{N_A}{1000\ cm^3}\times52000\times1.66\times10^{-24}\ g\times\frac{1}{24\times3600}\ day}=4.98\times10^8\ cm^3g^{-1}\,\mathrm{day}^{-1},$$

and

$$d_{Q_rQ}=\frac{3.0\times10^5}{\frac{N_A}{1000\ cm^3}\times25000\times1.66\times10^{-24}\ g\times\frac{1}{24\times3600}\ day}=1.04\times10^9\ cm^3g^{-1}\,\mathrm{day}^{-1},$$

where N_A is called the Avogadro number, and is the number of molecular per dm^3. $N_A=6.02\times10^{23}$, and 1.66×10^{-24} g is the mass of a proton for atomic mass unit.

Other parameters. The range of macrophages in the blood is $2\times10^{-5}-10^{-4}$ gcm^{-3} [75]; we take $M_0=5\times10^{-3}$ gcm^{-3}. The range of T cells in the blood is $0.5\times10^{-3}-1.5\times10^{-3}$ gcm^{-3} [49]; we take $T_0=1\times10^{-3}$ gcm^{-3}. The range of SMCs is $5\times10^{-3}-8\times10^{-3}$ gcm^{-3} [38]; we take $S_0=6\times10^{-3}$ gcm^{-3}. We assume that K_{Lox} is half of L_0 in Eq. (6), and similarly, $K_M=\frac{M_0}{2}$ in Eq. (7), and $K_F=\frac{M_0}{2}$ in Eq. (10). We assume that the influx of LDL and HDL into the intima is larger than the influx of macrophages and SMCs, and take $\alpha_L=\alpha_H=1.0$ cm^{-1}, and $\alpha_S=\alpha_M=0.2$ cm^{-1}. The influx of T cells is assumed to be smaller than that of macrophages, and we take $\alpha_T=0.05$ cm^{-1}.

Numerical methods

Finite element implementation. In order to illustrate our numerical method, we consider the following diffusion equation with Robin boundary conditions:

$$\frac{dX}{dt}+\gamma\nabla\cdot(\mathbf{u}X)-D\Delta X=f(X)\text{ in }\Omega,$$

$$\frac{\partial X}{\partial\mathbf{n}}+\alpha(X-X_I)=0\text{ on }\Gamma_I,\tag{27}$$

$$\frac{\partial X}{\partial\mathbf{n}}+\beta(X-X_M)=0\text{ on }\Gamma_M,$$

where $\gamma\nabla(\mathbf{u}X)$ is an advection term, and either $\gamma=1$ or $\gamma=0$ (no advection), and $\mathbf{u}=-\nabla\sigma$. Multiplying the differential equation by an arbitrary function v, and performing integration by parts using the boundary conditions, we get

$$\begin{aligned}&\int_\Omega\frac{dX}{dt}v dx+\gamma\int_\Omega X\nabla\sigma\cdot\nabla v dx+D\int_\Omega\nabla X\cdot\nabla v dx\\&=\int_\Omega f(X)v dx-\gamma\int_{\Gamma_I}Xv\frac{\partial\sigma}{\partial\mathbf{n}}ds-\int_{\Gamma_M}v\beta(X-X_M)ds\\&+\int_{\Gamma_I}v\alpha(X-X_I)ds.\end{aligned}\tag{28}$$

This is an equivalent formulation of the system (27), which is better suited for simulation.

Similarly, Eq. (21) for σ has the equivalent form:

$$\int_\Omega\nabla\sigma\cdot\nabla v dx-D\int_\Omega\nabla\rho\cdot\nabla v dx=\int_\Omega(\phi+\psi)v dx-\int_{\Gamma_M}v\frac{\partial\rho}{\partial n}ds,\tag{29}$$

for an arbitrary function v.

Galerkin discretization. The standard Galerkin discretization method uses finite dimensional subspaces V_h to approximate the solution X. Let $\{\omega_i\}_{i=1}^N$ be a basis of V_h, where N is the number of nodes within the triangulation K. Let $X_h^n\in V_h$ denote the numerical approximation of X at time $t=ndt$, where dt is the time step, X_h^n is written as a sum

$$X_h^n=\sum_{j=1}^N c_j^n\omega_j,\tag{30}$$

for coefficient c_j^n to be determined. If $\frac{\partial X}{\partial t}$ is approximated by $\frac{X^{n+1}-X^n}{dt}$, then (28) is equivalent to

$$\begin{aligned}&\int_\Omega(X^{n+1}-X^n)\omega_i dx+dt[\gamma\int_\Omega X^n\nabla\sigma\cdot\nabla\omega_i dx+D\int_\Omega\nabla X^{n+1}\cdot\nabla\omega_i dx]\\&=dt(\int_\Omega f(X^n)\omega_i dx-\gamma\int_{\Gamma_I}X^n\omega_i\frac{\partial\sigma}{\partial\mathbf{n}}ds\\&-\int_{\Gamma_M}\omega_i\beta(X^n-X_M)ds+\int_{\Gamma_I}\omega_i\alpha(X^n-X_I)ds),\end{aligned}\tag{31}$$

or,

$$\begin{aligned}&\int_\Omega X^{n+1}\omega_i dx+dtD\int_\Omega\nabla X^{n+1}\cdot\nabla\omega_i dx\\&=\int_\Omega X^n\omega_i dx-\gamma dt\int_\Omega X^n\nabla\sigma\cdot\nabla\omega_i dx+dt\int_\Omega f(X^n)\omega_i dx\\&+dt\int_{\Gamma_I}\omega_i(\alpha(X^n-X_I)-\gamma X^n\frac{\partial\sigma}{\partial\mathbf{n}})ds-dt\int_{\Gamma_M}\omega_i\beta(X^n-X_M)ds.\end{aligned}\tag{32}$$

Table 5. Parameters' description and value.

Parameter	Description	Value
χ_C	chemotactic sensitivity parameter	$8.64\times10^{-1}\sim1.73\times10^{4}$ cm^5 g^{-1} day^{-1} [36,37] (10)*
χ_H	haptotaxis parameter	$8.64\times10^{-2}\sim8.64\times10^{4}$ cm^5 g^{-1} day^{-1} [36,37] (10^2)*
L_0	source/influx of LDL in blood	$7\times10^{-4}-1.9\times10^{-3}$ gcm^{-3} [25]
H_0	source/influx of HDL in blood	$4\times10^{-4}-6\times10^{-4}$ gcm^{-3} [25]
r_0	source/influx of free radical into intima	0.26 gcm^{-3} day^{-1} [34]
M_0	source/influx of macrophages from blood	5×10^{-5} gcm^{-3} [75]
T_0	source/influx of T cells into intima	1×10^{-3} gcm^{-3} [49]
S_0	source/influx of SMCs into intima	6×10^{-3} gcm^{-3} [71]
ρ_0	ECM density	1×10^{-3} gcm^{-3} [28]
P_0	MCP-1 concentration	3×10^{-10} [73]
G_0	PDGF concentration	1.5×10^{-8} [72]
α_L	influx rate of LDL into intima	1.0 cm^{-1} estimated
α_H	influx rate of HDL into intima	1.0 cm^{-1} estimated
$\tilde{\alpha}_M$	influx rate of macrophage into intima	0.2 cm^{-1} estimated
α_T	influx rate of T cells into intima	0.05 cm^{-1} estimated
$\tilde{\alpha}_S$	influx rate of of SMCs into intima	0.2 cm^{-1} estimated
K_{Lox}	ox-LDL saturation for production of MCP-1	0.5 gcm^{-3} [64] & estimated
K_M	macrophages saturation for activation of T cells	2.5×10^{-5} gcm^{-3} [75] & estimated
	and production of IL-12	
K_F	foam cells saturation for production of IL-12	2.5×10^{-5} gcm^{-3} [75] & estimated
K_{I_γ}	IFN-γ saturation for activation of macrophages	1×10^{-11} gcm^{-3} [39]
$K_{I_{12}}$	IFN-γ saturation for production of IL-12	7×10^{-11} gcm^{-3} [45]

* Values chosen in the simulation.

doi:10.1371/journal.pone.0090497.t005

Recalling (30), we can rewrite the system (32) as a linear system of equations

$$Ac^{n+1}=b, \tag{33}$$

where c^n is the vector of (c_j^n), and the coefficient matrix $A=(A_{ij})$ and the right-hand side $b=(b_i)$ are defined by

$$A_{ij}=\int_\Omega \nabla\omega_i\cdot\nabla\omega_j dx+dt\int_\Omega \omega_i\omega_j dx,$$

and

$$\begin{aligned} b_j=&\int_\Omega\sum_j(c_j^n\omega_j)\omega_i dx-\gamma dt\int_\Omega\sum_j(c_j^n\omega_j)\nabla\sigma\cdot\nabla\omega_i dx\\ &+dt\int_\Omega f(\sum_j(c_j^n\omega_j))\omega_i dx+dt\int_{\Gamma_I}\omega_i(\alpha(\sum_j(c_j^n\omega_j)-X_I)\\ &-\gamma X^n\frac{\partial\sigma}{\partial\mathbf{n}})ds-dt\int_{\Gamma_M}\omega_i\beta(\sum_j(c_j^n\omega_j)-X_M)ds. \end{aligned}$$

Similarly, setting $\sigma_h^n=\sum_{j=1}^N d_j^n\omega_j$, where σ_h^n is a numerical approximation of σ at time ndt, Eq. (29) can be written as follows

$$Bd^n=e, \tag{34}$$

where d^n is the vector (d_j^n), B is a matrix (B_{ij}), $B_{ij}=\int_\Omega\nabla\omega_i\cdot\nabla\omega_j dx$, and $e_j=D\int_\Omega(\nabla\rho\cdot\nabla\omega_j)dx+\int_\Omega(\phi+\psi)\omega_j dx-\int_{\Gamma_M}\omega_j\frac{\partial\rho}{\partial n}ds$.

Outline of the procedure. Suppose the domain $\Omega(t)$ has polygonal boundaries $\Gamma_I(t)$ and $\Gamma_O(t)$. Then we can cover the closure $\overline{\Omega(t)}$ of $\Omega(t)$ by a regular triangulation $\mathcal{T}$ of triangles, i.e., $\overline{\Omega(t)}=\bigcup_{T\in\mathcal{T}}T$ where each T is a closed triangle. The triangular mesh, which is a basic thing that Finite Elements requires, is generated by distmesh [50], which is a mesh generation tool implemented in MATLAB, and our algorithm is outlined in **Algorithm S1**. For the detailed implementations, such as: construct basis functions over the triangulation, assemble the stiffness matrix, etc, see references [51,52].

Results

Numerical simulation is initialized by a small formed plaque. (see Figs. 4, 5, 6). Five combined levels of LDL and HDL (L_0 and H_0) are tested for 300 days:

(a) $(L_0,H_0)=(190,40)$: a small plaque doubles in size at 300 days;

(b) $(L_0,H_0)=(150,45)$: a small plaque increases approximately 50% at 300 days;

(c) $(L_0,H_0)=(130,50)$: a small plaque remains small at 300 days;

(d) $(L_0,H_0)=(110,52)$: a small plaque decreases approximately 30% at 300 days;

(e) $(L_0,H_0)=(70,60)$: a small plaque almost disappear at 300 days.

Fig. 4 shows the growth of the plaque in case (a), Fig. 5 shows the shrinkage of the plaque in case (c), and Fig. 6 shows almost no plaque in case (e). In Fig. 7, the weight of the plaque, the summation of total cells, namely, $\int_\Omega (M+F+S+T)d\Omega$, is plotted for these five scenarios of combined levels of LDL and HDL. Similarly to Fig. 7, we show in **supporting information files** how the populations of macrophages, SMCs, foam cells and T cells, as well as the concentration of ox-LDL, IFN-γ and IL-12, vary for different levels of LDL and HDL shown in Figs. S1, S2, S3, S4, S5, S6, S7.

Fig. 8 shows a risk-map of plaque development. To create the risk-map, we divided the LDL axis by 121 equidistant points, i.e, $L_i=70+i$ $(i=0,\cdots,120)$, and divided the HDL axis by 21 equidistant points, i.e., $H_j=40+j$ $(j=0,\cdots,20)$. For each pair (L_i,H_j), we computed the weight of the plaque, $W(L_i,H_j)$ after 100 days on the domain shown in Fig. 3 (B), and formed the risk matrix

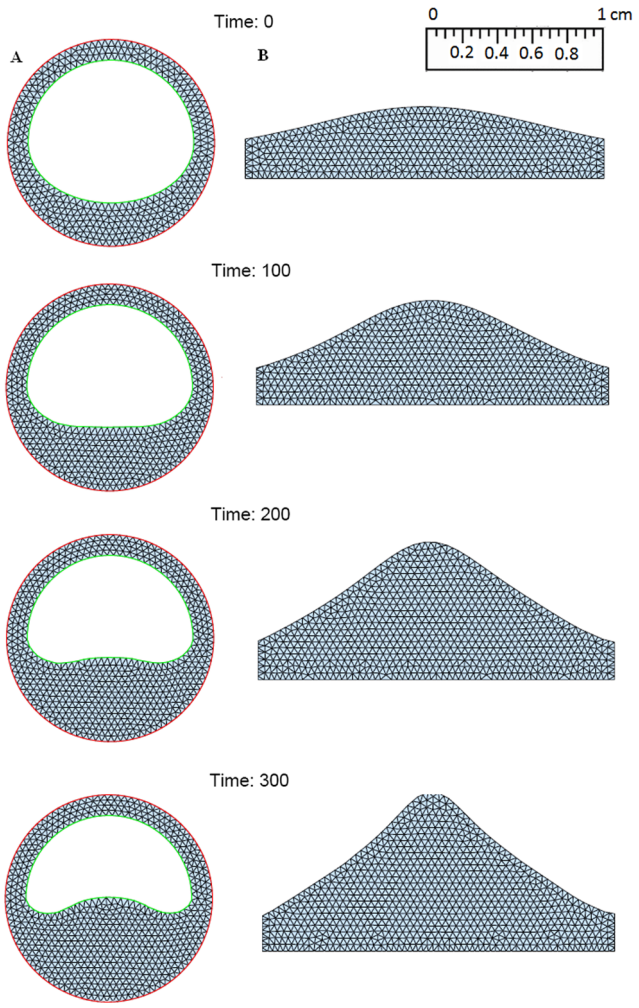

Figure 4. Simulations for the atherosclerosis model of 300 days after an initial plaque is formed with $H_0=40$ mg/dL and $L_0=190$ mg/dL. (A: Cross sections of a blood vessel, B:Cross sections along the blood vessel).
doi:10.1371/journal.pone.0090497.g004

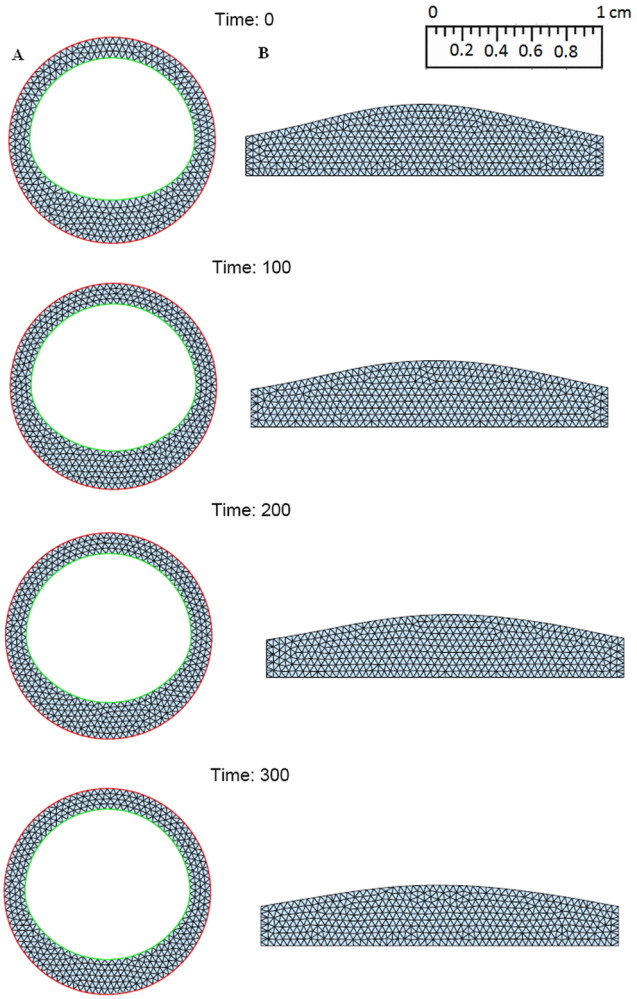

Figure 5. Simulations for the atherosclerosis model of 300 days after an initial plaque is formed with $H_0=50$ mg/dL and $L_0=130$ mg/dL. (A: Cross section of a blood vessel; B: Cross section along the blood vessel).
doi:10.1371/journal.pone.0090497.g005

$$A_{ij}=\frac{W(L_i,H_j)-W_0}{W_0},$$

where W_0 is the initial weight of the plaque. The vertical axis on the right of Fig. 8 shows the legend of the percentage of plaque growth or shrinkage. Accordingly, we divided the LDL-HDL plane into three regions: region I predicts high risk of plaque development, region III predicts no risk, and the intermediate region II predicts low risk.

Sensitivity analysis

In order to support the robustness of the simulation results, we ran sensitivity analysis on parameters which appear in the differential equations and in the boundary conditions. The parameters chosen are those whose baseline was somewhat crudely estimated while at the same time they seem to play an important role in the development of the plaque. Specifically, we chose all the 15 production rate parameters from the third box of Table 4, all the 5 influx rate parameters from the third box of

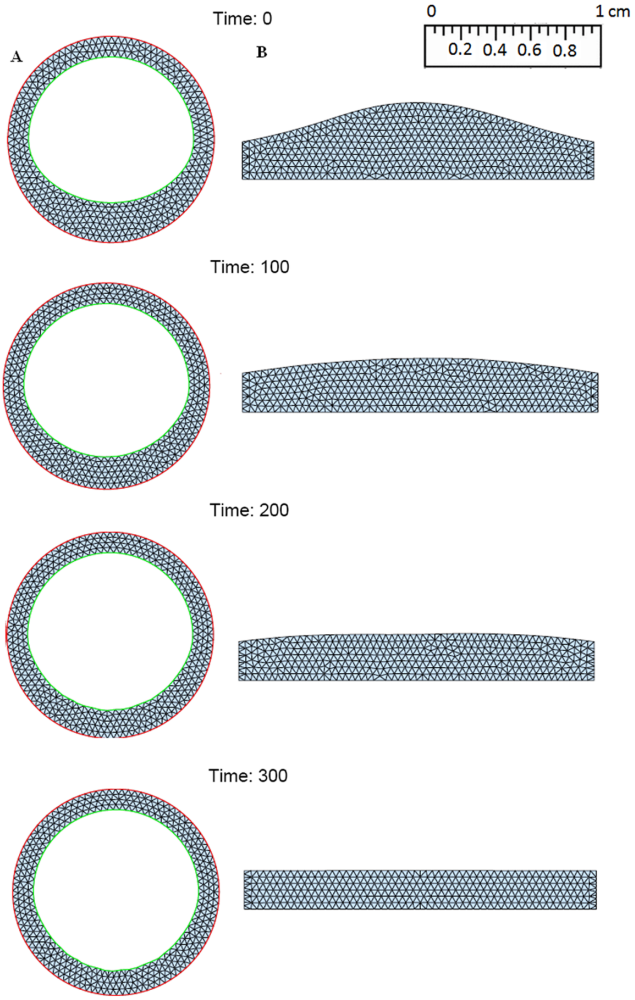

Figure 6. Simulations for the atherosclerosis model of 300 days after an initial plaque is formed with $H_0=60$ mg/dL and $L_0=70$ mg/dL. (A: Cross section of a blood vessel; B: Cross section along the blood vessel).
doi:10.1371/journal.pone.0090497.g006

Table 5, and L_0, H_0. We list all these parameters with their range, baseline and unit in Table 6.

Following the sensitivity analysis method described in [53], we performed Latin hypercube sampling and generated 100 samples to calculate the partial rank correlation coefficients (PRCC) and p-values with respect to the weight of the plaque after 300 days. The PRCCs are shown in Fig. 9, and all the p-values (not shown here) are less than 0.01. A positive PRCC (i.e., positive correlation) means that an increase in the parameter value will increase the weight of the plaque while a negative PRCC (i.e., negative correlation) means increase in the parameter will decrease the weight of the plaque. We note that λ_{QS} is positively correlated, as it should be. Indeed, if λ_{QS} is increased then MMP (Q) is increased (Eq. (12)) so that ECM (ρ) is decreased (Eq. (19)) and hence the plaque weight $\int(M+F+S+T)d\Omega$ is increased (Eq. (16)). As another example, note that $\lambda_{L_{ox}M}$ is negatively correlated. Indeed, if $\lambda_{L_{ox}M}$ is increased then L_{ox} is decreased (Eq. (3)), and α_M in the boundary condition will decrease, leading to smaller M, and then to smaller T and F. Similar explanation can be given to the other parameters.

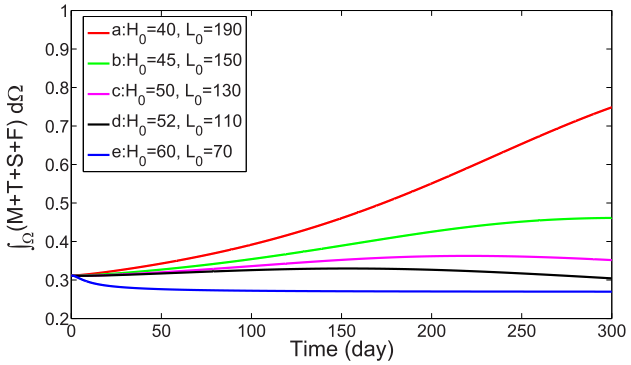

Figure 7. Plaque weights for different levels of LDL and HDL. The units of H_0 and L_0 are mg/dL.
doi:10.1371/journal.pone.0090497.g007

The most significant positively correlated parameters are L_0 and its influx rate α_L. This is not surprising since LDL initiates the plaque formation. The most significant negatively correlated parameters are H_0 and its influx rate α_H. Indeed, since HDL reduces the availability of free radicals, it plays an important negative role in plaque formation.

Discussion

Atherosclerosis is a disease in which a plaque builds up inside an artery. The process of plaque formation begins when, as a result of a lesion in the artery, cholesterols LDL and HDL enter the intima, and LDL becomes oxidized by free radicals. Upon sensing ox-LDL, endothelial cells secrete MCP-1 which attracts monocytes from the blood. As monocytes enter to the intima, they differentiate into macrophages that ingest the ox-LDL and become foam cells. Foam cells attract more macrophages, followed by T cells from the blood, and SMCs from the media. HDL reduces the available free radicals, as well as inflammation within the evolving plaque, thus HDL acts to block plaque growth.

Public health guidelines in the U.S. specify that LDL level of 100–129 mg/dL is near ideal, 130–159 mg/dL is borderline high, and 160–189 mg/dL is very high, whereas concentration of HDL above 60 mg/dL is best, and below 40 mg/dL for men or below 50 mg/dL for women is poor [25]. An important question is how to evaluate the risk of atherosclerosis for a pair of LDL and HDL taken together. This question is addressed in the present paper. We built a mathematical model of plaque development by a system of partial differential equations. The model includes two parameters: L_0, the level of LDL in the blood, and H_0, the the level of HDL in the blood.

The model can simulate the evolution of a small plaque for any pair of values of (L_0,H_0). In Figs. 4, 5, 6, we simulated the plaque evolution over a period of 300 days. For example, one extreme case of $L_0=190$ mg/dL, $H_0=40$ mg/dL, the plaque doubled after 300 days; in another extreme case of $L_0=70$ mg/dL, $H_0=60$ mg/dL, the plaque disappeared after 300 days. We created a risk-map by taking sampling points of LDL and HDL values, and computing the weight of the plaque for each pair (L_0,H_0) after 100 days. The map shown in Fig. 8, indicates the percentage of plaque growth or shrinkage for any such pair. We accordingly divided the (LDL,HDL) quadrant into three regions: high risk, low risk, and non risk.

The need to consider the ratio of LDL/HDL in predicting coronary heart disease was suggested in a case study by [54]. The American Heart Association considers the ratio $(Tc/HDL)>5$ to

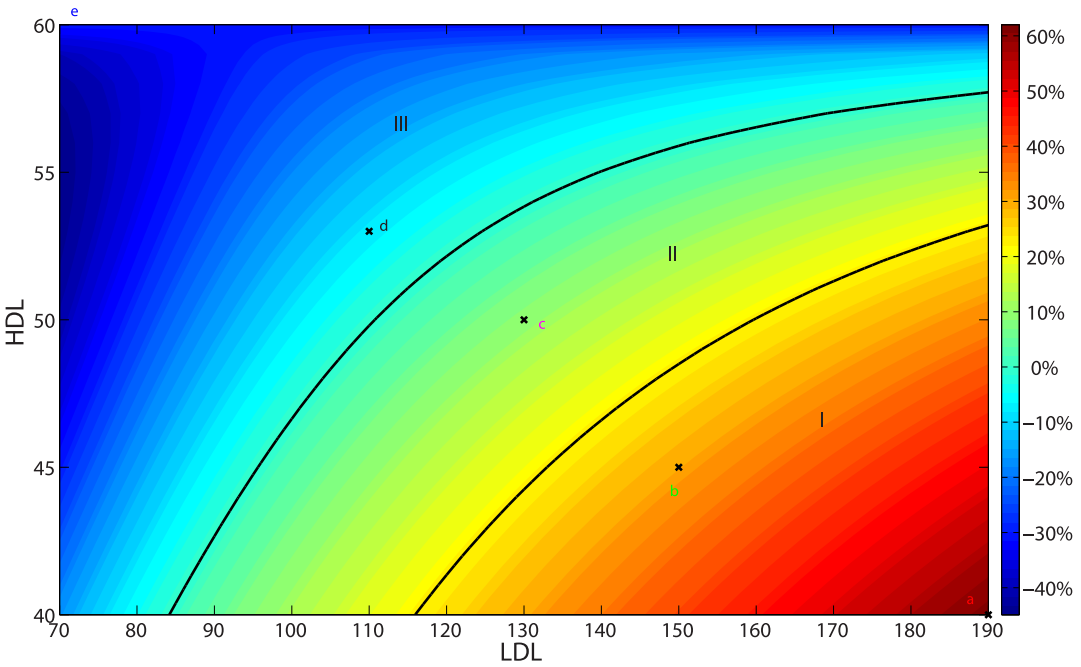

Figure 8. Risk map for plaque development: Region I high risk; Region II low risk; Region III no risk. The five points (L_i,H_j) whose plaque's weight was simulated in Fig. 7 over a period of 300 days are indicated by "x".
doi:10.1371/journal.pone.0090497.g008

Table 6. Parameters chosen for sensitivity analysis.

Parameter	Range	Baseline	Unit
$\lambda_{L_{ox}M}$	[5,20]	10	gcm^{-3} day^{-1}
λ_{MI_γ}	[0.002, 0.01]	0.005	day^{-1}
λ_{PE}	$[4.32\times10^{-10}, 1.73\times10^{-9}]$	8.65×10^{-10}	gcm^{-3} day^{-1}
$\lambda_{TI_{12}}$	$[5\times10^{5}, 2\times10^{6}]$	1×10^{6}	day^{-1}
$\lambda_{I,T}$	[0.033, 0.132]	0.066	day^{-1}
$\lambda_{I_{12}M}$	$[1.5\times10^{-7}, 6\times10^{-7}]$	3×10^{-7}	gcm^{-3} day^{-1}
$\lambda_{I_{12}F}$	$[5\times10^{-8}, 2\times10^{-7}]$	1×10^{-7}	gcm^{-3} day^{-1}
λ_{GM}	[0.05, 0.2]	0.1	day^{-1}
λ_{GF}	[0.016, 0.066]	0.033	day^{-1}
λ_{GS}	[0.25, 1]	0.5	day^{-1}
λ_{QS}	$[1.5\times10^{-4}, 6\times10^{-4}]$	3×10^{-4}	day^{-1}
$\lambda_{Q,S}$	$[1.5\times10^{-5}, 6\times10^{-5}]$	3×10^{-5}	day^{-1}
$\lambda_{Q,M}$	$[3\times10^{-5}, 1.2\times10^{-4}]$	6×10^{-5}	day^{-1}
λ_{ρ}	[0.266, 0.864]	0.432	day^{-1}
λ_{FM}	[0.06, 0.24]	0.12	day^{-1}
α_L	[0.5, 2.0]	1.0	cm^{-1}
α_H	[0.5, 2.0]	1.0	cm^{-1}
$\tilde{\alpha}_M$	[0.1, 0.4]	0.2	cm^{-1}
α_T	[0.025, 0.1]	0.05	cm^{-1}
$\tilde{\alpha}_S$	[0.1, 0.4]	0.2	cm^{-1}
L_0	$[5\times10^{-4}, 2\times10^{-3}]$	1×10^{-3}	gcm^{-3}
H_0	$[2\times10^{-4}, 8\times10^{-4}]$	5×10^{-4}	gcm^{-3}

doi:10.1371/journal.pone.0090497.t006

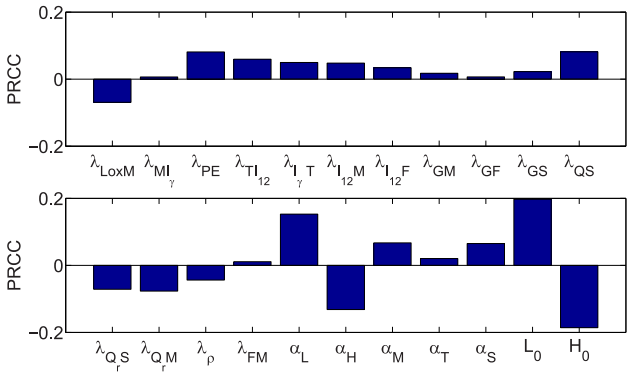

Figure 9. The PRCC of parameters for sensitivity analysis.
doi:10.1371/journal.pone.0090497.g009

indicate high risk of heart disease, and the ratio $(Tc/HDL)<3.5$ to be risk free [55], where Tc denotes the total cholesterol, which is calculated by the formula

$$Tc=LDL+HDL+\frac{1}{5}Tr\ \ (Tr=\text{triglycerides}).$$

Table 7 shows the National Cholesterol Education Program (NCEP) guidelines associated with plaque buildup [56]. Accordingly, for the five points (a)–(e) in **Results** we have:

(a) $\frac{Tc}{HDL}>5$ for any value of Tr;
(b) $\frac{Tc}{HDL}>5$ if Tr is above normal;
(c) $3.5<\frac{Tc}{HDL}<5$ if Tr is not very high;
(d) $\frac{Tc}{HDL}<3.5$ if Tr is normal;
(e) $\frac{Tc}{HDL}<2.5$ if Tr is normal;.

According to the NCEP guidelines, (a) and (b) should be in the high risk region; (c) in the low risk region; and (d), (e) in the no risk region, as indeed they are according placed in the risk map in Fig. 8.

Some anti-cholesterol drugs, such as statins, lower LDL and at the same time also increase the HDL [24]. It is important to know which drugs can best achieve the desired risk-free balance between LDL and HDL, that is, bring the individual's (L_0,H_0) into the no risk (or low risk) region. By focusing not on just reducing L_0 or on just increasing H_0, but on moving the combined (L_0,H_0) to the no risk (or low risk) region in the shortest medically feasible path, we believe one could choose a more personalized medicine from those currently available, which will reduce the risk of atherosclerosis with the lowest amount of doze, thereby also possibly reducing potential negative side effects.

To illustrate this approach, we note that for some drugs the ratio of decrease in LDL to increase in HDL is already known. For example, this ratio is 1/3 for the new experimental drug *Evacetrapib*. Some anti-cholesterol drugs only decrease LDL (e.g. Colestid) while others only increase HDL (e.g. Lofibra). We can the represent effect of such drugs by unit vectors in the (L_0,H_0) plane: for example, Colestid $\leftarrow$, Lofibra $\uparrow$, and Evacetrapid $\nwarrow$. In Fig. 10. we consider three individuals, A, B, and C in the high risk region. In order to move them to the low risk region with the minimum amount of medication (side effects are ignored), the individual should choose the drug for which the line segment from the individual initial position to the low risk region is the shortest (We assume that the amount of drug is proportional to the length of the line segment). Thus the best drug for A is the one that primarily increases HDL. Similarly, C will do better with a drug that primarily decrease LDL, and B should use a drug with appropriate ratio of decreasing LDL to increasing HDL.

Some work has been done on antioxidant therapy for reducing the risk of atherosclerosis, but so far it has had limited success in preventing cardiovascular diseases [57–59]. A review of studies in which antioxidant gene therapy has been successfully used is given in [60]. Our model could account for antioxidative medication once we gain a good understanding of how such medication affects the source of free radicals, r_0, in Eq. (4).

Table 7. National Cholesterol Education Program guidelines.

LDL Cholesterol Level	**Category**
Less than 100 mg/dL	Optimal
100 to 129 mg/dL	Near or above optimal
130 to 159 mg/dL	Borderline high
160 to 189 mg/dL	High
190 mg/dL and above	Very high
HDL Cholesterol Level	**Category**
Less than 40 mg/dL (for men)	Low HDL cholesterol.
Less than 50 mg/dL (for women)	A major risk factor for heart disease.
60 mg/dL and above	High HDL cholesterol.
Triglyceride Level	**Category**
Less than 100 mg/dL	Optimal
Less than 150 mg/dL	Normal
150–199 mg/dL	Borderline high
200–499 mg/dL	High
500 mg/dL and above	Very high

doi:10.1371/journal.pone.0090497.t007

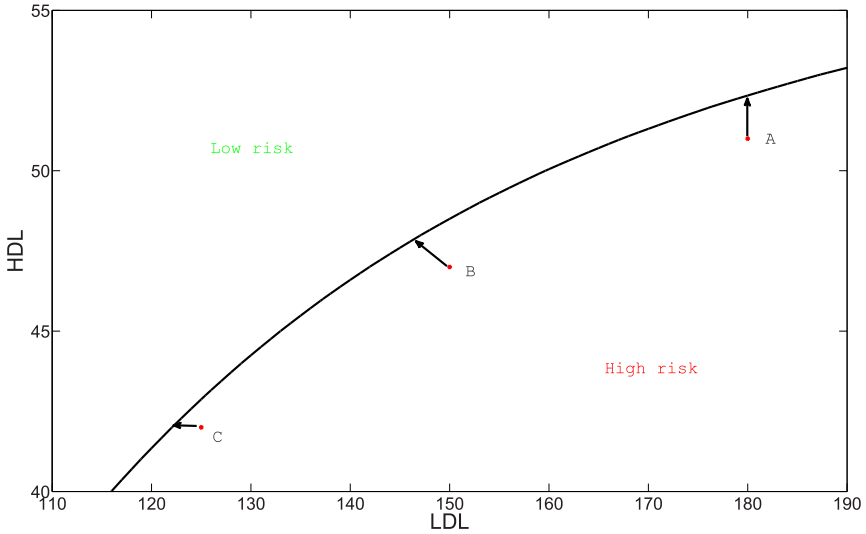

Figure 10. Drug treatment recommended for individuals A, B and C.
doi:10.1371/journal.pone.0090497.g010

Some of the parameters in the differential equations in our model had to be rather crudely estimated, since no data were available, while others may slightly vary depending on the individual. As more data become available, parameter values may be further refined. Our model uses only the values of LDL and HDL as biomarkers. It will be interesting in the future to incorporate also triglycerides into the risk-map. Future work should also explore how other risk factors, such as high blood pressure, smoking and diabetes affect the risk-map.

We did not include in this paper the circulation ox-LDL in the blood, which is elevated only in patients with advanced atherosclerosis [61,62]. Our model could be extended to include this additional biomarker, but at present there is not enough data on how the level of ox-LDL in the blood correlates to a specific advanced state of the disease.

Supporting Information

Algorithm S1 Algorithm for finite element implementation of the mathematical model.
(PDF)

Figure S1 Macrophages population for different levels of LDL and HDL.
(PDF)

Figure S2 SMCs population for different levels of LDL and HDL.
(PDF)

Figure S3 T cells population for different levels of LDL and HDL.
(PDF)

Figure S4 Foam cells population for different levels of LDL and HDL.
(PDF)

Figure S5 Concentration of ox-LDL for different levels of LDL and HDL.
(PDF)

Figure S6 Concentration of IFN-γ for different levels of LDL and HDL.
(PDF)

Figure S7 Concentration of IL-12 for different levels of LDL and HDL.
(PDF)

Author Contributions

Contributed reagents/materials/analysis tools: WH AF. Wrote the paper: WH AF.

References

1. Hoyert DL, Xu J (2012) Deaths: Preliminary Data for 2011, National Vital Statistics Reports 61.
2. The top 10 causes of death. Available: http://www.who.int/mediacentre/factsheets/fs310/en/. Accessed 2013 Dec. 18.
3. Frink RJ (2002) Inflammatory Atherosclerosis, Heart Research Foundation.
4. Moreno PR (2010) Vulnerable Plaque: Definition, Diagnosis, and Treatment. Cardiology Clinics 28: 1–30.
5. Libby P, Ridker PM, Maseri A (2002) Inflammation and Atherosclerosis. Circulation 105: 1135–1143.
6. Cohen A, Myerscough MR, Thompson RS (2012) Athero-protective effects of High Density Lipoproteins (HDL): An ODE model of the early stages of atherosclerosis. Preprint.
7. McKay C, McKee S, Mottram N, Mulholland T, Wilson S (2005) Towards a model of atherosclerosis. Strathclyde Mathematics Research Report.
8. Ryu BH (2000) Low Density Lipoprotein (LDL), Atherosclerosis and Antioxidants. Biotechnol. Bioprocess Eng. 5: 313–319.
9. Harrington JR (2000) The Role of MCP-1 in Atherosclerosis. Stem Cells 18: 65–66.
10. Reape TJ, Groot P (1999) Chemokines and atherosclerosis. Atherosclerosis 147: 213C225.
11. Osterud B, Bjorklid E (2003) Role of Monocytes in Atherogenesis. Physiol Rev. 83: 1069–1112.
12. Gui T, Shimokado A, Sun Y, Akasaka T, Muragaki Y (2012) Diverse Roles ofMacrophages in Atherosclerosis: From Inflammatory Biology to Biomarker Discovery. Mediators of Inflammation 2012: ID693083.
13. Johnson JL, Newby AC (2009) Macrophage heterogeneity in atherosclerotic plaques. Curr Opin Lipidol.20: 370–378.
14. Little MP, Gola A, Tzoulaki I (2009) A Model of Cardiovascular Disease Giving a Plausible Mechanism for the Effect of Fractionated Low-Dose Ionizing Radiation Exposure. PLoS Computational Biology 5: e1000539.
15. Calvez V, Ebde A, Meunier N, Raoult A (2009) Mathematical modelling of the atherosclerotic plaque formation. CEMRACS 2008 - Modelling and Numerical Simulation of Complex Fluids 28: 1–12.
16. Ross R, Masuda J, Raines EW, Gown AM, Katsuda S, et al. (1990) Localization of PDGF-B protein in macrophages in all phases of atherogenesis. Science 248: 1009–1012.

17. Raines EW, Ross R. (1993) Smooth muscle cells and the pathogenesis of the lesions of atherosclerosis. Br Heart J. 69: 30–37.
18. Rodriguez JA, Orbe J, Paramo JA (2007) Metalloproteases, Vascular Remodeling, and Atherothrombotic Syndromes. Rev Esp Cardiol 60: 959–967.
19. Fabunmi RP, Sukhova GK, Sugiyama S, Libby P (1998) Expression of Tissue Inhibitor of Metalloproteinases-3 in Human Atheroma and Regulation in Lesion-Associated Cells A Potential Protective Mechanism in Plaque Stability. Circ Res. 83: 270–278.
20. King IL, Segal BM (2005) Cutting edge: IL-12 induces CD4+CD25- T cell activation in the presence of T regulatory cells. J Immunol. 175: 641–645.
21. Hansson GK, Holm J, Jonasson L (1989) Detection of activated T lymphocytes in the human atherosclerotic plaque, Am. J Pathol. 135: 169–175.
22. Kosaka C, Masuda J, Shimokado K, Zen K, Yokota T, et al. (1992) Interferon-gamma suppresses PDGF production from THP-1 cells and blood monocyte-derived macrophages. Atherosclerosis 97: 75–87.
23. Barter P (2005) The role of HDL-cholesterol in preventing atherosclerotic disease, European Heart Journal Supplements. 7: 4–8.
24. Barter P, Brandrup-Wognsen G, Palmer M, Nicholls S (2010) Effect of statins on HDL-C: a complex process unrelated to changes in LDL-C: analysis of the VOYAGER Database. J Lipid Res. 51: 1546–1553.
25. Mayo Clinic Staff, Cholesterol levels: What numbers should you aim for? Available: http://www.mayoclinic.com/health/cholesterol-levels/CL00001. Accessed 2013 Dec. 12.
26. Rahdert DA, Sweet WL, Tio FO, Janicki C, Duggan DM (1999) Measurement of density and calcium in human atherosclerotic plaque and implications for arterial brachytherapy. Cardiovasc Radiat Med. 1: 358–367.
27. Orbe J, Rodriguez JA, Arias R (2003) Antioxidant vitamins increase the collagen content and reduce MMP-1 in a porcine model of atherosclerosis: Implications for plaque stabilization. Atherosclerosis 167: 45–53.
28. Kim Y, Roh S, Lawler S, Friedman A (2011) miR and AMPK mutual antagonism in glioma cell migration and proliferation: a mathematical model. PLoS One 6: e28293.
29. Byrne HM (1997) The importance of intercellular adhesion in the development of carcinomas. IMA Journal of Mathematics Applied in Medicine & Biology 14: 305–323.
30. Byrne HM (1999) A weakly nonlinear analysis of a model of avascular solid tumour growth. J Math Biol. 39: 59–89.
31. Byrne HM, Chaplain MA (1996) Modelling the role of cell-cell adhesion in the growth and development of carcinomas. Mathematical and Computer Modelling 24: 1–7.
32. Chothia C (1976) The nature of the accessible and buried surfaces in proteins. J Mol Biol. 105: 1–12.
33. Janin J, Chothia C (1978) Role of Hydrophobicity in the Binding of Coenzymes. Biochemistry 17: 2943–2948.
34. Cobbold C, Sherratt J, Maxwell S (2002) Lipoprotein oxidation and its significance for atherosclerosis: a mathematical approach. Bulletin of Mathematical Biology 64: 65–95.
35. Ingold KU, Bowry VW, Stocker R, Walling C (1993) Autoxidation of lipids and antioxidation by a-tocopherol and ubiquinol in homogeneous solution and in aqueous dispersions of lipids: unrecognised consequences of lipid particle size as exemplified by oxidation of human low density lipoprotein. Proc Natl Acad Sci. 90: 45–49.
36. Kim Y, Lawler S, Nowicki M, Chiocca E, Friedman A (2009) A mathematical model for pattern formation of glioma cells outside the tumor spheroid core. J Theor Biol. 260: 359–371.
37. Kim Y, Friedman A (2010) Interaction of tumor with its micro-environment: A mathematical model. Bull Math Biol. 75: 1029–1068.
38. Mercapide J, Cicco R, Castresana J, Klein-Szanto A (2003) 450 Stromelysin-1/matrix metalloproteinase-3 (MMP-3) expression accounts for invasive properties of human astrocytoma cell lines. Int J Cancer 106: 676–682.
39. Friedman A, Turner J, Szomolay B (2008) A model on the influence of age on immunity to infection with Mycobacterium tuberculosis. Exp Gerontol 43: 275–285.
40. Orme IM (1987) Aging and immunity to tuberculosis: increased susceptibility of old mice reflects a decreased capacity to generate mediator T lymphocytes. J Immunol. 138: 4414–4418.
41. Barrett T, Benditt E (1988) Platelet-derived growth factor gene expression in human atherosclerotic plaques and normal artery wall. Proc Natl Acad Sci. 85: 2810–2814.
42. Xue C, Friedman A, Sen CK (2009) A mathematical model of ischemic cutaneous wounds. Proc Natl Acad Sci. 106: 16782–16787.
43. Dollery CM, Libby P (2006) Atherosclerosis and proteinase activation. Cardiovascular Research 69: 625–635.
44. Chen D, Roda JM, Mash CB, Eubank TD, Friedman A (2012) Hypoxia inducible factors mediated-inhibition of cancer by GM-CSF: A mathematical model. Bulletin of Mathematical Biology 74: 2752–2777.
45. Day J, Friedman A, Schlesinger LS (2009) Modeling the immune rheostat of macrophages in the lung in response to infection. Proc Natl Acad Sci. 106: 11246–11251.
46. Yamamoto S, Nguyen JH (2006) TIMP-1/MMP-9 imbalance in brain edema in rats with fulminant hepatic failure. J Surg Res. 134: 307–314.
47. Olson MW, Gervasi DC, Mobashery S, Fridman R (1997) Kinetic analysis of the binding of human matrix metalloproteinase-2 and -9 to tissue inhibitor of metalloproteinase (TIMP)-1 and TIMP-2. J Biol Chem. 21: 29975–29983.
48. Palosaari H, Yliopisto O (2003) Matrix Metalloproteinases (MMPs) and Their Specific Tissue Inhibitors (TIMPs) in Mature Human Odontoblasts and Pulp Tissue. Oulun yliopisto.
49. Bofill M, Janossy G, Lee CA, MacDonald-Burns D, Phillips AN, et al. (1992) Laboratory 475 control values for CD4 and CD8 T lymphocytes Implications for HIV-1 diagnosis. Clin Exp Immunol. 88: 243–252.
50. Persson PO, Strang G (2004) A Simple Mesh Generator in MATLAB. SIAM Review 46: 329–345.
51. Alberty J, Carstensen C, Funken SA (1999) Remarks around 50 lines of Matlab: short finite element implementation. Numerical Algorithms 20: 117–137.
52. Z Li. The finite element method for two dimensional problems. Chapter 9 Avialable http://www4.ncsu.edu/~zhilin/TEACHING/MA587/chap9.pdf. Accessed 2013 Oct. 10.
53. Marino S, Hogue IB, Ray CJ, Kirschner DE (2008) A methodology for performing global uncertainty and sensitivity analysisin systems. J Theor Biol. 254:178–196.
54. Arsenault BJ, Rana JS, Stroes ES, Despres JP, Shah PK, et al. (2009) Beyond low-density lipoprotein cholesterol: respective contributions of non-high-density lipoprotein cholesterol levels, triglycerides, and the total cholesterol/high-density lipoprotein cholesterol ratio to coronary heart disease risk in apparently healthy men and women. J Am Coll Cardiol. 55:35–41.
55. Mayo Clinic Staff, How important is cholesterol ratio? Available: http://www.mayoclinic.org/diseases-conditions/high-blood-cholesterol/expert-answers/cholesterol-ratio/faq-20058006. Accessed 2013 Dec. 20.
56. Crestor Managing Cholesterol. Available: http://www.crestor.com/c/your-arteries/tools-resources/index.aspx
57. Otani H (2013) Site-Specific Antioxidative Therapy for Prevention of Atherosclerosis and Cardiovascular Disease. Oxid Med Cell Longev.
58. Ozkanlar S, Akcay F (2012) Antioxidant vitamins in atherosclerosis–animal experiments and clinical studies. Adv Clin Exp Med. 21: 115–123.
59. Tardif J (2005) Antioxidants and atherosclerosis: emerging drug therapies. Curr Atheroscler Rep. 7: 71–77.
60. Levonen A, Vahakangas E, Koponen JK, Herttuala S (2008) Antioxidant Gene Therapy for Cardiovascular Disease Current Status and Future Perspectives. Circulation 117: 2142–2150.
61. Ishigaki Y, Oka Y, Katagiri H (2009) Circulating oxidized LDL: a biomarker and 501 a pathogenic factor. Curr Opin Lipidol 20: 363–369.
62. Tsimikas S, Witztum JL (2001) Measuring circulating oxidized low-density lipoprotein to evaluate coronary risk. Circulation 103: 1930–1932.
63. Rajman I, Eacho P, Chowienczyk P, Ritter J (1999) LDL particle size: an important drug target? Br J Clin Pharmacol 48: 125–133.
64. Hokland B, Mendez A, Oram J (1992) Cellular localization and characterization of proteins that bind high density lipoprotein. J Lipid Res. 33: 1335–1342.
65. Mitsuhashi T, Ono K, Fukuda M, Hasegawa Y (2013) Free radical scavenging ability and structure of a 90-kDa protein from the scallop shell. Fisheries Science 79: 495–502.
66. Garcia-Tunon I, Ricote M, Ruiz A, Fraile B, Paniagua R, et al. (2007) Influence of IFN-gamma and its receptors in human breast cancer. BMC Cancer 7: 158.
67. Antoniades H (1981) Human platelet-derived growth factor (PDGF): purification of PDGF-I and PDGF-II and separation of their reduced subunits. Proc Natl Acad Sci. 78: 7314–7317.
68. Yokochi S, Hashimoto H, Ishiwata Y, Shimokawa H, Haino M, et al. (2001) An Anti-Inflammatory Drug, Propagermanium, May Target GPI-Anchored Proteins Associated with an MCP-1 Receptor, CCR2. Journal of Interferon and Cytokine Research 21: 389–398.
69. Hamza T, Barnett J, Li B (2010) Interleukin 12 a Key Immunoregulatory Cytokine in Infection Applications. Int J Mol Sci. 11: 789–806.
70. O'Keefe JH, Cordain L, Harris WH, Moe RM, Vogel R (2004) Optimal low-density lipoprotein is 50 to 70 mg/dl: lower is better and physiologically normal. Journal of the American College of Cardiology 43: 2142–2146.
71. Miller DC, Thapa A, Haberstroh KM, Webster TJ (2004) Endothelial and vascular smooth muscle cell function on poly(lactic-co-glycolic acid) with nano-structured surface features. Biomaterials 25: 53–61.
72. Bowen-Pope DF, Malpass TW, Foster DM, Ross R (1984) Platelet-derived growth factor in 526 vivo: levels, activity, and rate of clearance. Blood 64: 458–469.
73. Rhodes J, Sharkey J, Andrews P (2009) Serum IL-8 and MCP-1 concentration do not identify patients with enlarging contusions after traumatic brain injury. J Trauma 66: 1591–1597.
74. Gattorno M, Picco P, Vignola S, Stalla F, Buoncompagni A, et al. (1998) Serum interleukin 12 concentration in juvenile chronic arthritis. Ann Rheum Dis. 57: 425–428.
75. Tietz NW (1999) Clinical Guide to Laboratory Tests. Philadelphia 3rd Ed.
76. Liao KL, Bai XF, Friedman A (2013) The role of CD200-CD200R in tumor immune evasion. J Theor Biol. 328: 65–76.
77. Tsukaguchi K, Balaji KN, Boom WH (1995) CD4+ alpha beta T cell and gamma delta T cell responses to Mycobacterium tuberculosis. J Immunol, 154: 1786–1796.